EDITORIAL CSIC

Materiales de Construcción
76 (361), January-March 2026, e402
ISSN-L: 0465-2746, eISSN: 1988-3226
https://doi.org/10.3989/mc.2026.394225

ARTICLE

Printability of stabilized solids for low cement consumption blocks

Imprimibilidad de sólidos estabilizados para bloques de bajo consumo de cemento

F. M. Lima
Postgraduate Program in Civil and Environmental Engineering (PPCIVAM), Federal University of Rio Grande do Norte, (Natal, Brazil)
Corresponding author: fernandalima0106@gmail.com, https://orcid.org/0009-0009-8151-2000

M. A. S. dos Anjos
Postgraduate Program in Civil and Environmental Engineering (PPCIVAM), Federal University of Rio Grande do Norte, (Natal, Brazil); Postgraduate Program in Civil and Environmental Engineering (PPGECAM), Federal University of Paraíba, (João Pessoa, Brazil)
marcos.anjos@ifpb.edu.br, https://orcid.org/0000-0001-9563-2534

I. M. S. Barros
Postgraduate Program in Civil and Environmental Engineering (PPGECAM), Federal University of Paraíba, (João Pessoa, Brazil)
ilana.barros@academico.ufpb.br, https://orcid.org/0000-0002-8719-6055

U. S. Nunes
Postgraduate Program in Civil and Environmental Engineering (PPCIVAM), Federal University of Rio Grande do Norte, (Natal, Brazil)
uesleisilvanunes3@gmail.com, https://orcid.org/0000-0001-9534-9632

Abstract: This paper investigates the use of sandy silt in 3D printing by stabilizing it with Portland cement and chemical additives (metakaolin and limestone filler). The goal is to make the soil compatible with the 3D printing process and ensure pumpability. The experimental program began with a reference mixture of soil to cement in a 1:1 mass ratio to achieve a consistency suitable for the extrusion method. The study also examined the content of chemical additives, the water-to-dry material ratio, printing speed, and nozzle height conditions. The analysis included the reduction of cement in two mixtures, T15%C and T20%C, with mass proportions of 0.15:0.85:1 and 0.2:0.80:1. It was confirmed that soil-cement blocks could be successfully produced with compressive strengths of 3.1 MPa and 3.0 MPa for the T15%C and T20%C compositions, respectively, indicating a cement reduction of 87% and 82% compared to the reference mixture (REFT100).

Keywords: 3D printing; Additive manufacturing; Earth construction; Constructability.

Resumen: Este artículo investiga el uso de suelo arenoso en la impresión 3D mediante su estabilización con cemento Portland y adiciones minerales (metacaolín y relleno de piedra caliza). El objetivo es hacer que el suelo sea compatible con el proceso de impresión 3D y garantizar la bombeabilidad. El programa experimental comenzó con una mezcla de referencia de suelo a cemento en una proporción de masa de 1:1 para lograr una consistencia adecuada para el método de extrusión. El estudio también examinó el contenido de aditivos químicos, la proporción de agua a material seco, la velocidad de impresión y las condiciones de altura de la boquilla.El análisis incluyó la reducción de cemento en dos mezclas, T15%C y T20%C, con proporciones de masa de 0.15:0.85:1 y 0.2:0.80:1. Se confirmó que se podían producir con éxito bloques de suelo-cemento con resistencias a la compresión de 3,1 MPa y 3,0 MPa para las composiciones T15%C y T20%C, respectivamente, indicando una reducción de cemento del 87% y 82% respecto a la mezcla de referencia (REFT100).

Palabras clave: Impresión 3D; Fabricación aditiva; Construcción en tierra; Constructibilidad.

Received: 03-09-2025 / **Accepted**: 14-02-2025 / **Published**: 25-06-2026

Citation: Lima FM, Anjos MAS, Barros IMS, Nunes US. 2026. Printability of stabilized solids for low cement consumption blocks. *Mater. Construcc.* 76 (361): e402. https://doi.org/10.3989/mc.2026.394224

Supplementary information ↓

1. INTRODUCTION

The building and construction sector contributes around 21% of global greenhouse gas emissions and generates 25% of the world's solid waste. This places considerable pressure on the sector to minimize its impact and explore new material solutions that utilize low-impact mineral resources (1-3). The choice of building materials significantly influences a building's overall energy consumption and carbon footprint. To minimize these impacts, it's essential to prioritize efficient materials and construction methods that reduce material use and waste generation. For instance, utilizing natural clays sourced locally can help minimize environmental impacts (4).

Earthen construction is among the oldest and most prevalent vernacular construction methods. Throughout history, three main traditional construction techniques have been developed: adobe, taipa, and cob. The cob technique is characterized by the construction of monolithic walls built with moist, malleable soil without the use of formwork (5). In the 3D printing process, wet methods are the most suitable, which is why the adobe and cob techniques are the most researched (6).

It's important to note that while traditional techniques provide a solid foundation for integrating earthen construction with 3D printing, specific adjustments must be made to account for the rheology of earthen mixtures as they relate to various types of printing systems and construction geometries. These adjustments are essential to enhance printing capabilities, minimize cracking, and improve layer stacking capacity.

The earth utilized for construction is typically sourced from the vicinity where the structures will be erected. It naturally contains clay, which serves as a binding agent, but in some cases, this material may not be suitable for the 3D printing process. As a result, additional components such as fine sand, alternative types of clay, and fibers are often incorporated to ensure that the composite material maintains optimal consistency and extrusion continuity (7, 8).

Several studies, including those by Perrot *et al.* (9), Bajpayee *et al.* (4), Gomaa *et al.* (10), Ferretti *et al.* (5), Faleschini *et al.* (6), have focused on developing alternative construction materials to replace conventional ones. Their aim is to create sustainable technologies that reduce waste in the construction process through additive manufacturing.

When considering rheological properties, it is crucial to emphasize the significance of viscosity and fluidity in 3D printing. These properties are influenced by the ratio of paste volume to aggregate volume (11). The paste plays a vital role in ensuring cohesion while maintaining the partial separation of aggregate particles. Additionally, it acts as a lubricant, reducing friction forces and facilitating the smooth flow of the system (11-13).

Even though extensive studies have been conducted on the use of 3D printing in cementitious materials and the factors affecting bonding between layers, the 3D printing of earth-based materials continues to pose challenges for existing printing systems. These challenges include material grain size, properties of the materials, mixing ratios, and the incorporation of local organic fibers. Addressing these challenges will require thorough experimental research before a construction method with suitable technical feasibility can be developed (10).

3D printing with earth is still in the early stages of development. In 2016, the Italian company WASP achieved a milestone by 3D printing the first life-size earth structure (6). Subsequently, in 2017, TerraPerfoma and researchers from the Institute of Advanced Architecture of Catalonia (IAAC) collaborated to construct the first full-size 3D-printed clay wall, focusing on achieving good thermal performance and structural integrity (14). The following year, a group of IAAC students demonstrated the material's versatility by expanding the 3D wall to 5 meters high and 2 meters wide, incorporating a staircase and upper floor slab with a wooden structure (14, 15).

In 2018, the companies WASP and Rice House unveiled the world's first fully 3D-printed earth house, called the "Gaia House," utilizing their updated system, Crane WASP©. The house was printed on-site using a combination of soil, water, rice straw, rice husks, and lime. For improved insulation, rice straw filled internal voids in the walls, and wooden structures supported the roof's construction loads (14). Concurrently, in France, researchers Perrot, Rangeard, and Couteille (9) studied using a 3D printer with a fast-setting binder made from seaweed biopolymers known as alginate. This project was the first published paper to explore the mechanical properties and structural performance of 3D earth-based material (14), revealing the ability to print earth-based mortar with compressive strength equivalent to conventional cob earth (9, 14).

In 2019, IAAC and the company WASP conducted a study on the load-bearing capabilities of a 3D-printed adobe wall. They constructed a wooden staircase with floors installed across the printed wall to test its ability to support the staircase and withstand regular use. In 2021, the company WASP introduced TECLA, its largest 3D earth construction project. TECLA aimed to create a new home printed in 3D using two printers simultaneously, featuring a dome structure to eliminate the excess roof structure observed in 2018 (14).

Scientific research has explored mixtures for 3D printing using earth, incorporating lime and cement stabilizers, as well as natural stabilizers like alginate and potato starch. These mixtures may also include mineral additions, fibers, and additives. Noteworthy works include those of D'Haese *et al.* (16), who used approximate earth material to cement proportions of 1:0.43 and 1:0.25, along with a retarder additive. D'Haese *et al.* (17) developed various mass proportions, ranging from 1:1 to 1:0.25 (soil:cement), replacing part of the cement with fly ash. Faleschini *et al.* (6) employed 8 to 11% cement of the total mixture weight, with mass proportions ranging from 1:0.17 to 1:0.12 (soil:cement), and also included additions like rice husk, marble dust, and solid waste incinerator ash. Additionally, Soda et. al (18) created mixtures with proportions of 1:0.50 and 1:0.35 (soil:cement), incorporating blast furnace slag and superplasticizing and viscosity modifying additives.

Recent studies have focused on soil-cement printing, with less emphasis on research in Brazil. This investigation aims to assess the printability of soil-cement mixtures with varying levels of cement replaced by metakaolin and limestone filler while maintaining consistent amounts of superplasticizer (SP) and viscosity-modifying additive (HPMC). The performance of the soil-cement mixtures will be evaluated in terms of printability and through tests in both fresh and hardened states.

2. MATERIALS AND METHODS

2.1. Materials

The following materials were utilized to prepare the mixtures for 3D printing soil-cement: 1) Portland cement CP-V of high initial strength (CPV, similar to ASTM Type II); 2) Soil collected from the metropolitan region of Natal-RN/Brazil; 3) Metakaolin (MK, HP ULTRA); 4) Limestone filler (LF dolomitic); 5) Superplasticizer additive (SP, MGLENIUM); 6) Viscosity-modifying additive based on hydroxypropylmethylcellulose (HPMC); 7) Mixing water from the local utility company. Figure 1 illustrates images of the materials used in the research, including a) Soil, b) Portland Cement CP-V, c) Metakaolin, and d) Limestone filler.

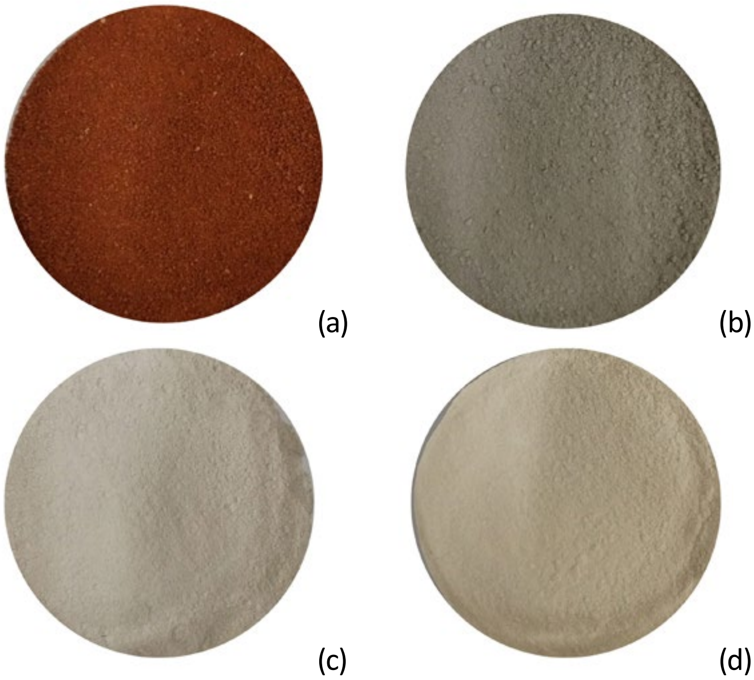

Figure 1. (a) Soil, (b) Portland Cement CP-V, (c) Metakaolin, and (d) Limestone filler.

In order to classify the soil, a particle size test was performed according to the standard ABNT, NBR 7181 (19). This test produced the graph displayed in Figure 2, which includes the particle size curves of other dry materials like Portland Cement CP-V, metakaolin, and limestone filler.

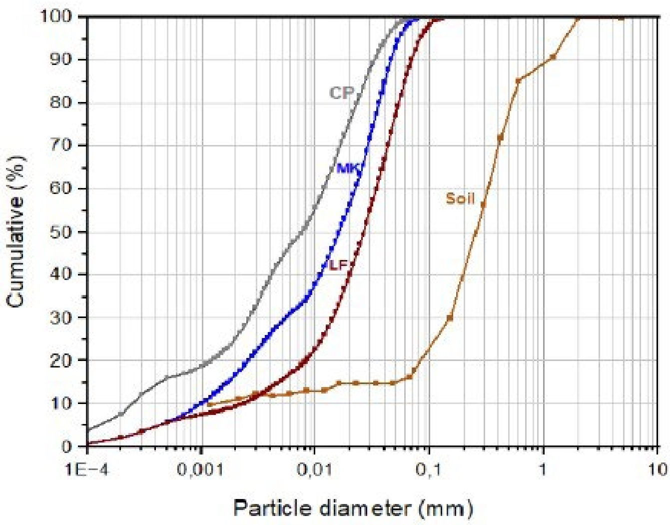

Figure 2. Particle size distribution curve of cement, metakaolin, limestone filler, and soil.

Based on the particle size analysis and in accordance with the Unified Soil Classification System (USCS), the soil is categorized as coarse-grained because only 18.04% of the material passed through the 0.075 mm sieve. Additionally, as no material was retained on the 4.8 mm sieve, this soil can be classified as sandy.

Regarding the secondary characteristics of the soil, it is not possible to obtain results according to the classification system procedure because the soil lacks the plasticity needed to reach the liquidity limit (LL) and, consequently, the plasticity index (IP). This indicates that the soil does not contain clay particles that contribute to this plasticity; therefore, it can be classified as sandy silty.

According to the results from the particle size analysis, Table 1 shows the physical properties of the materials, corresponding to the through-diameter values (d10, d50, and d90). These values are statistical indicators extracted directly from the cumulative particle size distribution, representing the particle sizes at which 10%, 50%, and 90% of the total particles are found, measured in micrometers (µm).

Table 1. Physical properties of cement, soil, metakaolin, and limestone filler.

Physical properties	CP-V	Soil	MK	LF
Through-diameter (d10) (µm)	0.23	1.20	0.96	2.63
Through-diameter (d50) (µm)	7.33	250.0	16.07	26.60
Through-diameter (d90) (µm)	12.38	1220	45.78	69.53

In preparation for the printing system, the soil underwent a drying process in an oven at 105ºC for 24 hours and was then filtered through a No. 16 ABNT sieve (1.18 mm). The authors chose to use the portion of soil that passed through this sieve, in line with previous research findings by Araújo (20) and Diniz *et al.* (21). Table 2 presents the physical properties—specific weight and unit weight—of the soil, cement, metakaolin, and filler limestone, measured in grams per cubic centimeter (g/cm³), these measurements adhered to established Brazilian standards: NBR NM 52 (22), NBR NM 53 (23), and NBR NM 45 (24).

Table 2. Physical properties of cement, soil, metakaolin and limestone fíller and technical standards.

Physical properties	Technical standards	CP-V	Soil	MK	LF
Specific weight (g/cm³)	(NBR NM 52), (NBR NM 53)	3.09	2.65	2.65	2.78
Unit weight (g/cm³)	(NBR NM 45)	1.33	1.29	0.72	1.90

2.2. X-Ray Fluorescence Spectrometry (XRF) chemical analysis of soil, Portland Cement CP-V, metakaolin, and limestone filler

The soil samples, Portland cement V, metakaolin, and limestone filler underwent analysis using a Bruker S2 Ranger apparatus at the Molecular Sieves Laboratory—LABPEMOL/UFRN. The analysis was conducted with Pd anode radiation, utilizing a maximum power of 50 W, a maximum voltage of 50kV, and a maximum current of 2 mA, with an XFlash® Silicon Drift Detector. The results of the chemical analysis, along with the percentages of oxides for CP-V, MK, and LF, are detailed in Table 3.

Table 3. Chemical analysis of soil and fine materials.

Oxides (%)	SiO_2	Fe_2O_3	Al_2O_3	TiO_2	K_2O	CaO	ZrO_2	SO_3	P_2O_5	MgO	CuO	Cr_2O_3	Others
Soil	66.84	14.30	11.28	4.33	1.22	0.74	0.41	0.24	0.23	-	0.07	0.04	0.30
CP-V	12.48	3.15	3.41	0.29	2.13	69.70	-	6.46	0.46	1.2	-	-	1.18
MK	66.25	2.99	25.05	2.39	0.47	0.12	0.10	0.12	-	1.2	-	0.03	1.28
LF	12.85	2.16	4.33	0.38	1.68	67.54	0.01	-	-	8.5	-	-	2.55

2.3. Proportions of the mixtures

The experimental program was developed based on an initial empirical analysis of mixtures using a 3D printer for cementitious materials at UFRN. Diniz *et al.* (21), noted that the variation in paste volume/aggregate volume (Vp/Va) ranged from 1.81 to 0.81, with a volume ratio of 1:0.8 to 1:1.8. On the other hand, Araújo (20) obtained a Vp/Va variation of 1.69 to 1.27, with volume proportions ranging from 1:0.84 to 1:1.06. In this research, the volume of paste (Vp) per volume of soil (Vs) ranged from 3.19 to 2.47, maintaining a mass ratio of 1:1 for the mixtures. The mass proportion was converted into volume to quantify the total volume to be printed. Next, the substitution of sand for soil was analyzed.

Despite the Portland cement content resulting in high consumption for the printer's mixtures, which is atypical for a soil mix, it was necessary to consider adapting the locally available soil to enable printing using soil:cement mixtures in a 1:1 mass ratio. This adjustment is essential to provide the required pumping capacity and buildability based on the available conditions.

Given the potential to use the soil in the specified proportion for printing, it was determined that replacing the cement with mineral additives of suitable viscosity would be beneficial. This substitution is intended to decrease the amount of cement while ensuring that the paste volume remains conducive to pumping and printing, especially since the soil in question is not ideal due to its low clay content.

In accordance with the specified ratio, water content, superplasticizer, and HPMC were tested for 3D printing. The printing was conducted using a gantry-type printer with a print area measuring 100 cm in width, 100 cm in length, and 50 cm in height. The printer (Figure 3) is equipped with a pumping system and a 20 mm diameter nozzle, integrated with a 3-axis printing system controlled by stepper motors and software. For pumping, a 3 HP motor, along with a frequency inverter, transports the material through a 19 mm diameter hose to the print nozzle at a speed of 80 mm/s and with a deposition height of 1 cm.

Figure 3. 3D printer.

In reference to the original mixture (REFT100) with a 1:1 (soil:cement) mass ratio, we examined mixtures with reduced cement consumption. In the research, it was essential to consider adapting locally available soil for printing by using mixtures with similar mass ratio (1:1) of soil:cement or soil:(cement+MK+LF).This involved replacing 80% and 85% of the cement, by mass, with mineral additions (20% metakaolin and 60% or 65% limestone filler), resulting in compositions T20%C and T15%C, respectively. We assessed the printability of the T20%C and T15%C mixtures by adjusting the ratio of the water-to-dry material (W/DMaterials = water / (CP + LF + MK + SOIL)) while maintaining a constant percentage of HPMC and SP additives across all mixtures. We achieved a suitable consistency for printing by varying the water ratio.

Throughout the mixing process, we followed these steps: incorporation of the dry materials, addition of the HPMC additive with 15% water, mixing with 60% water, addition of the superplasticizer, and finally, adding the remaining 25% water. Material consumption was calculated in kg/m^3 based on the specific masses of the respective materials used.

The printing capacity (pumping and building) of 3DCP mixtures is controlled by the volume of paste and the granular material/binder ratio (11). Metakaolin and limestone filler were used to partially replace cement, resulting in a small difference in the paste volume/soil volume ratio (Vp/Vsoil) for the T15%C and T20%C mixtures and a more considerable difference in the reference mixture (REFT100).

In this study, the fines were defined as the cumulative mass of cement, soil particles smaller than 0.074 mm, metakaolin (MK), and limestone filler (LF). The paste volume (Vp) is determined by the sum of the volume of Portland Cement (CP-V), the volume of mineral additions (MK and LF), and the volume of water, as outlined in Table 4, which refers to the composition of the soil-cement mixtures. The Vp/Vsoil ratio was determined as the volume of paste divided by the volume of soil. Thus, the T15%C and T20%C mixtures have higher Vp due to the inclusion of MK and LF, which represents a higher content of fines (material passing the 0.075 mm sieve) and consequently a greater demand for water to obtain a consistency suitable for printing.

Table 4. Composition of soil-cement mixtures.

Mixtures	Mass ratio (1:1) CPV	Soil	MK	FC	Water/ Cement	SP (%)	HPMC (%)	W/ DMaterials	W/ Fines	Paste Volume (dm³)	Paste Volume/ Soil Volume	Cement Consumption (kg/m³)
REFT100	1	1	-	-	0.44	0.50	0.15	0.22	0.37	0.76	2.02	876.44
T15%C	1	6.67	1.33	4.33	3.93	0.50	0.15	0.29	0.50	6.29	2.50	113.60
T20%C	1	5	1	3	2.90	0.50	0.15	0.29	0.49	4.66	2.47	152.78

2.4. Tests on fresh soil-cement mixtures

The fresh state analysis measured the spread on the ABNT NBR 13276, consistency table (25). The test consisted of filling a metallic conical mold in three layers with 15, 10, and 5 blows using a metallic rod. Subsequently, the mold was removed, and the consistency table was activated, causing 30 drops in 30 seconds. The test concluded with the measurement of the spread and obtaining the consistency index ABNT NBR 13276 (25). This test was conducted to determine the water content in the soil-cement mixtures REFT100, T15%C, and T20%C to obtain consistency between 190 ± 25 mm. Additionally, the "sac-a-poche" method, as proposed by Faleschini *et al.* (6), was implemented to simulate the extrusion process prior to printing. This method serves as a preliminary analysis technique to verify the successful formation of layers and their stacking behavior. Moreover, the assessment of buildability was performed to determine the maximum number of layers that could be printed before structural failure occurred, according to ISO/ASTM 52939 (26). The experimental methodology is further elucidated in Figure 4, which delineates the sequential phases of the research process.

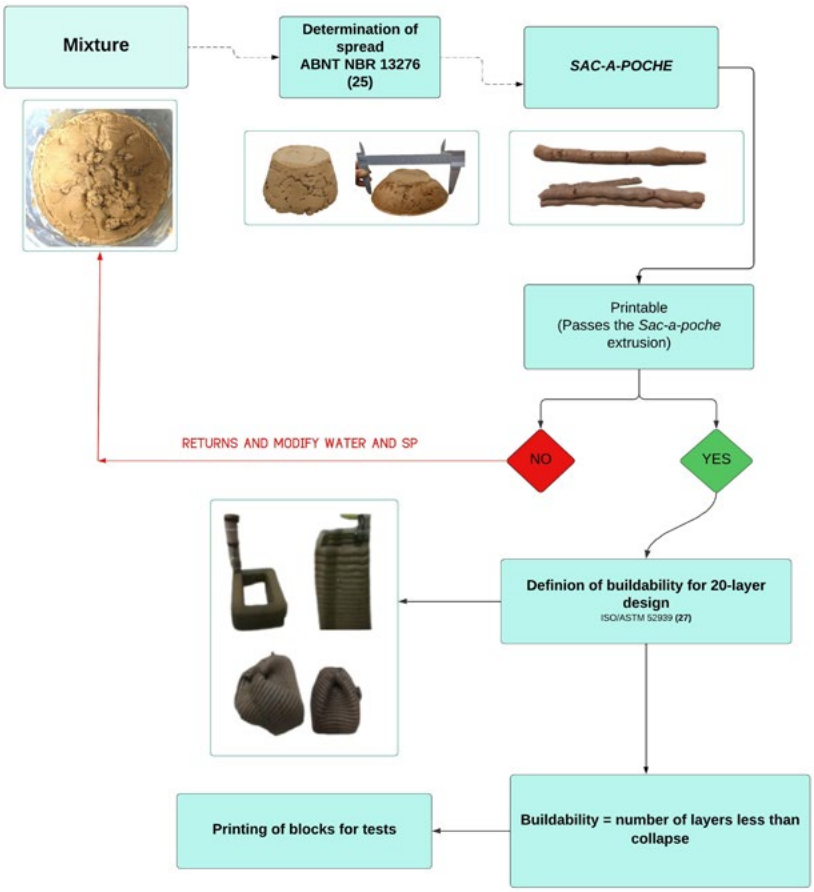

Figure 4. Experimental process flowchart.

2.5. Tests on the hardened state of soil-cement mixtures

2.5.1. Analysis of the Dimensions of Printed Soil-Cement Blocks

A dimensional analysis was performed on three blocks printed with each of the mixtures REFT100, T15%C, and T20%C. This analysis aimed to evaluate the quality and uniformity of the material. The blocks had dimensions of 140 mm x 190 mm x 160 mm, and the analysis was conducted after the blocks had cured for 28 days in a humid chamber. The analysis involved assessing two parameters: lateral deviation about a leveled square and dimensional variation in relation to the 3D model designed. This dimensional analysis is also recommended in the ABNT NBR 8492 Standard (27) to evaluate the quality of pressed soil-cement blocks. To measure the lateral deviation, the blocks were leveled with reference to a square, and the distances of the layers from the square were then measured with a caliper, as shown in Figure 5.

(a) (b)

Figure 5. Determining the lateral deviation with a square (a) left view, and (b) right view.

Dimensional variation refers to the disparities between the predetermined dimensions of the designed model and the final printed object. This is assessed in terms of length (C), width (L), and height (H) as illustrated in Figure 6. Each dimension was measured twice on both sides (left and right) at layers 4, 8, and 12, using a caliper with a precision of 0.05 mm.

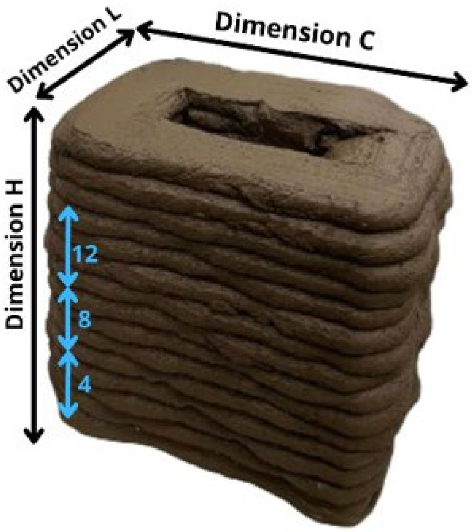

Figure 6. Example of the dimensions taken from the soil-cement block (REFT100).

2.5.2. Compressive strength of printed soil-cement blocks

In conducting the compressive strength test, we utilized a servo-controlled press with a loading speed of 0.05 MPa/s. The test was specifically performed on blocks as recommended by Nunes *et al.* (28) to assess the strength of mixtures for 3D printing masonry. To simulate the walls, we evaluated a reduced element with a shape resembling half a masonry block, mirroring the geometric characteristics of the intended wall layers up to a maximum stacking capacity of 16 layers (refer to Figure 7).

(a) (b)

Figure 7. Compressive strength test of printed soil-cement blocks (a) block capping before the test and (b) block compressive strength test.

2.5.3. Compressive strength and flexural tensile strength of parts extracted from printing

The compressive strength and flexural tensile strength were determined in accordance with the ABNT NBR 13279 Standard (29), using three samples of prismatic specimens measuring 40 mm x 40 mm x 160 mm. These samples were extracted from the cured block after 28 days and then cut using a machine with a diamond blade. They were coated with plaster and tested in two directions, X and Y, with a loading speed of 500 ± 50 N/s, as illustrated in Figure 8. An example of the specimens after cutting and testing in the X and Y axes is shown in Figure 9.

(a) (b)

Figure 8. Cutting the blocks to obtain the test pieces (a) representation of the cut in the fx direction and (b) representation of the cut in the fy direction.

2.5.4. Immersion water absorption, void ratio, and specific mass of test specimens

The assessment for water absorption through immersion, void ratio, and specific mass of the specimens in their solidified state at 28 days adheres to the guidelines outlined in ABNT NBR 9778 (30). However, we made modifications to the process to adhere to standard recommendations for the duration in the oven and immersion in water, totaling 72 hours each. Due to concerns about potential material disintegration, we chose to shorten each stage by one day, resulting in placing the three prismatic samples (40x40x160 mm) in the oven for 48 hours and immersion in water for 48 hours. The outcomes of the mechanical tests conducted in this study are detailed in Table 5.

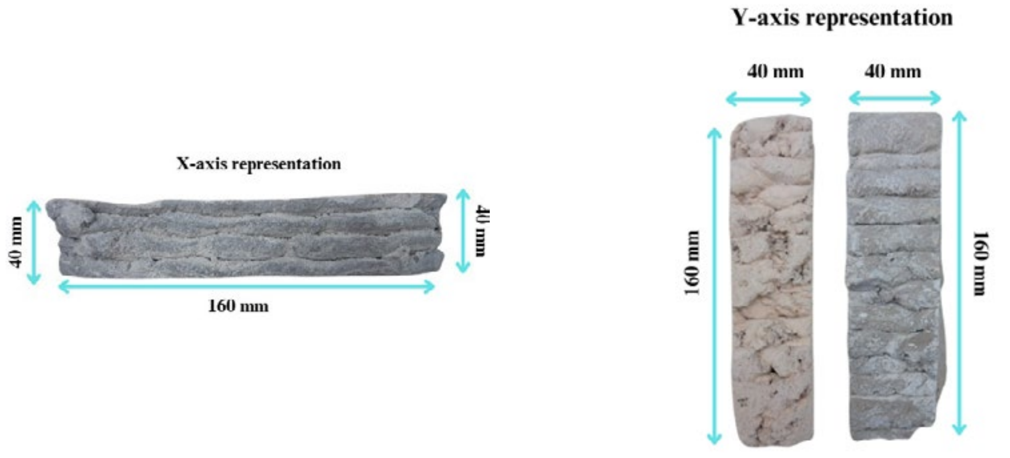

(a) (b)

Figure 9. Representation of the parts cut on the X and Y axes: (a) representation of the cut on the x-axis with dimensions 40x40x160 mm; (b) representation of the cut on the y-axis with dimensions 40x40x160 mm.

Table 5. Diagram of the mechanical tests performed.

Tests	Standard	Sample sizes (mm)	Quantity	Age of samples (days)
Dimensional analysis	-	140x190x160	3	28
Compressive strength	NBR 13279 (2005)	140x190x160	3	28
Compressive and tensile flexural strength	NBR 13279 (2005)	40x40x160	3	28
Immersion water absorption	NBR 9778 (2009)	40x40x160	3	28
Void ratio	NBR 9778 (2009)	40x40x160	3	28
Specific mass	NBR 9778 (2009)	40x40x160	3	28

3. RESULTS AND DISCUSSION

3.1. Chemical analysis of soil and fine materials

In several analyses conducted by Lahbabi *et al.* (31); Soda *et al.* (18); Faleschini *et al.* (6) and Silva *et al.* (32), it was found that the predominant oxides in the soil samples are silica (SiO_2), iron (Fe_2O_3), and alumina (Al_2O_3).

Soda *et al.* (18) presented XRF results indicating that the soil consists of 53.10% silica (SiO_2), 33.90% alumina (Al_2O_3), and 9.39% iron (Fe_2O_3), classifying it as a medium plasticity clay soil with 42.5% clay content and 16% plasticity index. Faleschini *et al.* (6) stated that the soil they examined contains 42.4% silica (SiO_2). Silva *et al.* (32) reported that the base soil had a high silica (SiO_2) content of 58.6%, 15.6% alumina (Al_2O_3), and 6.4% iron (Fe_2O_3), along with a liquidity limit of 27.0% and a plasticity index of 16.2%. Lahbabi *et al.* (31) found that the S and T soils they studied were rich in silica (60%), alumina (14%), and iron (7%) and suggested that the oxides of silica (SiO_2) and alumina (Al_2O_3) contribute to the strength of the final construction product.

Several authors, including Davey, Russell, Wilson, (33) and Muñoz V. *et al.* (34), Boukili *et al.* (35), Gol *et al.* (36), and Lahbabi *et al.* (31), have underscored the potential impact of iron oxide (Fe_2O_3) on color. In their research, the significant percentages of iron (Fe_2O_3) (14.30%) and titanium (TiO_2) (4.33%) in the soil justify its red color, as seen in table 3.

3.2. Fresh characteristics

Figures 10a, 10b, and 10c illustrate the fresh state tests of the REFT100, T15%C, and T20%C mixtures, while Figures 10d, 10e, and 10f depict the spreading measurements (in millimeters). Additionally, Figure 11 presents the results of the consistency index (mm), paste volume (dm³), and cement consumption (kg/m³).

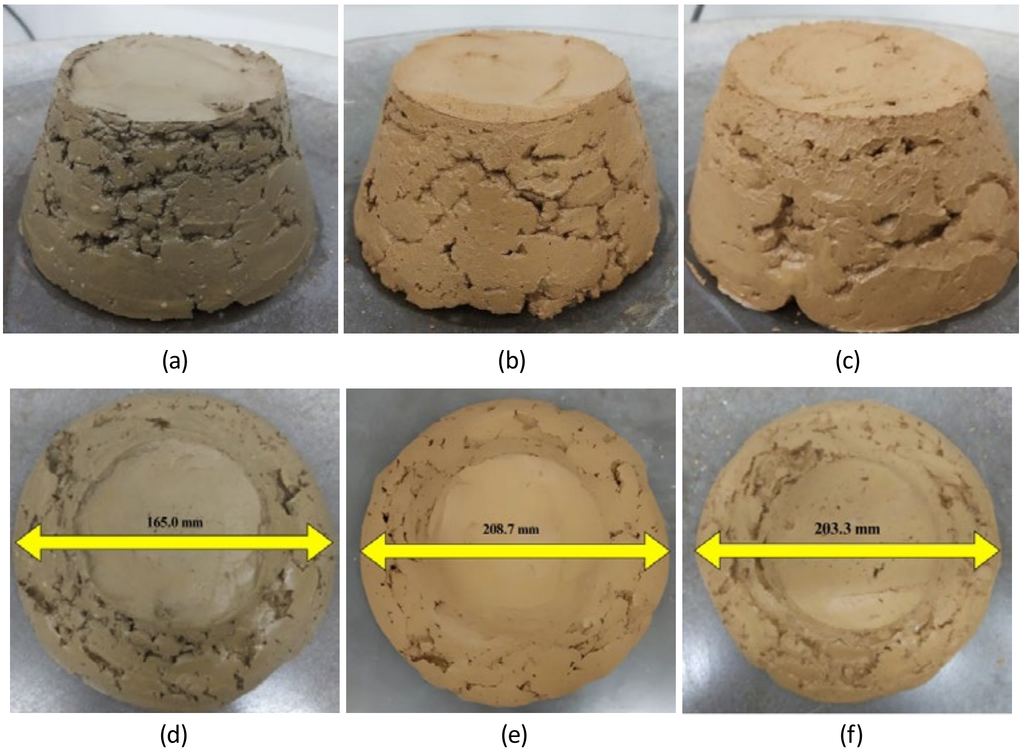

Figure 10. Fresh tests (a) reference mix mold, (b) T15%C mix mold, (c) T20%C mix mold, (d) reference mix spread, (e) T15%C mix spread, and (f) T20%C mix spread.

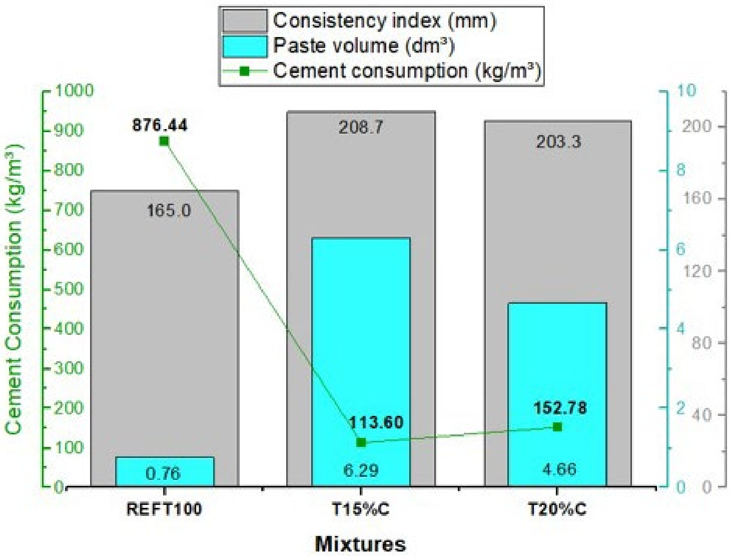

Figure 11. Consistency index, paste volume, and cement consumption.

The results indicate that the reference mixture has the lowest consistency index among the mixtures analyzed with metakaolin and limestone filler. The increased spreading of the mixtures with additions, such as T15%C and T20%C, is attributed to the higher paste volume value, which is a result of the increased water required (W/DMaterials) for the wetting of the earth and fine particles. These particles are crucial for achieving suitable spreading levels (160-210 mm) for printing.

According to Tay, Qian, and Tan, (37), a slump flow between 150 and 190 mm results in a smooth surface with high buildability. The printable region of the material can be determined based on the slump-flow values on the consistency table. Ma, Li, and Wang, (38), found that spreading from 174 to 210 mm allows the mixture to be printable. However, Dias *et al.* (11) noted that the appropriate spreads depend on the printing system to be used, including the type of extrusion, nozzle, and pumping.

When substituting cement with filler and metakaolin, a higher water demand is necessary to facilitate printing and ensure the required fluidity and extrusion of the mixture. However, increasing water content reduces the construction capacity in terms of layer deformation. This increased water demand is particularly evident as the percentage of Portland Cement replaced by mineral additions, such as metakaolin and limestone filler, rises due to a higher proportion of fine materials (39-41).

Mineral additions play a critical role in modifying the cohesion and consistency of fresh cement mixtures, mainly when their average particle diameters are smaller than those of Portland Cement, as is the case with metakaolin. The lamellar structure of metakaolin not only increase the viscosity of the mixture but also tends to increase the water content compared to mixtures containing spherical mineral particles. Its incorporation as a mineral component in high-performance cement is primarily justified by its exceptional pozzolanic activity, and imparts unique benefits related to durability and mechanical performance, while concurrently reducing overall cement consumption.

The spreading test is commonly employed to assess the fresh state properties of the mixture. However, spreading provides a good indication of whether the mixtures have the right consistency for printing. In this work, spreading was combined with "*sac-a-poche*" to assess the possibility of printing before testing on the printer. In this paper, we examined the printing parameters integral to the functioning of a 3-axis printing system, specifically focusing on the pumping mechanism and nozzle configuration, both of which are driven by stepper motors and controlled via specialized software.

3.3. Buildability analysis

Based on the fresh state tests shown in Figure 12, the vertical and lateral stability under increasing loads from overlapping layers (buildability) was defined as the number of stacking layers obtained in the mixtures under analysis. Observations of the impression of the mixtures indicated a sharp increase in impression failures starting at the 17th layer and culminating in structural collapse at the 19th layer (Figure 12).

Consequently, a threshold of 16 layers was established as the standardized limit for all printed blends evaluated in this investigation, which is marginally below the maximum permissible collapse threshold of the reference blend as identified through buildability analysis. This suggests that the substitution of cement with metakaolin and fillers in the ratios examined in this research does not adversely affect the buildability of the mixtures. Figure 12 illustrates the preliminary analysis of the buildability associated with the 1:1 reference mixture (soil:cement).

(a) (b) (c) (d)

Figure 12. Buildability: 19-layer print attempt (a), beginning of print (b) Composite with 19-layer print failure, (c) 19-layer collapse with side view and (d) 19-layer collapse with front view.

It's important to note that the 3D printing system used in the research requires a significant amount of cement in the mixtures, as confirmed in the results of Diniz *et al.* (21), Araújo *et al.* (42), and in the reference result of this work. To achieve similar results using soil for 3D printing, it's necessary to explore alternative materials that can replace cement and exhibit comparable viscosity and paste volume/volume soil. In other words, the aim is to obtain results similar to those obtained with the reference mixtures while maintaining constant additive contents, including superplasticizer and HPMC, across all mixtures.

The findings indicate that mixtures with reduced cement content exhibit compromised buildability when compared to higher cement content mixtures. This reduction in buildability is attributed to the increased demand for water, which is necessary to achieve optimal viscosity. Reduction in buildability was attributed in a visual assessment, which showed the printed layers looking flawed in the T15%C and T20%C mixes, this being associated with the increased demand for water needed. This assessment was confirmed in the dimensional assessment tests presented in section 3.4.1, especially in terms of height, where the REFT100 mixture showed less variation between the projected height and the actual height.

3.4. Characteristics in the hardened state

3.4.1. Evaluation of the dimensional analysis of soil-cement blocks

The research findings indicate that there is no linear relationship in the percentage variation among the analyzed mixtures. With respect to width (L), the percentage variation in the actual dimension was minimal for the reference and T15%C mixtures, but more significant for the T20%C mixture. In terms of length (C), only the T15%C mixture showed a smaller percentage variation, while both the reference and T20%C mixtures exhibited a greater variation and were more similar. Figure 13 illustrates the results of measuring the percentage variation of the printed soil-cement blocks.

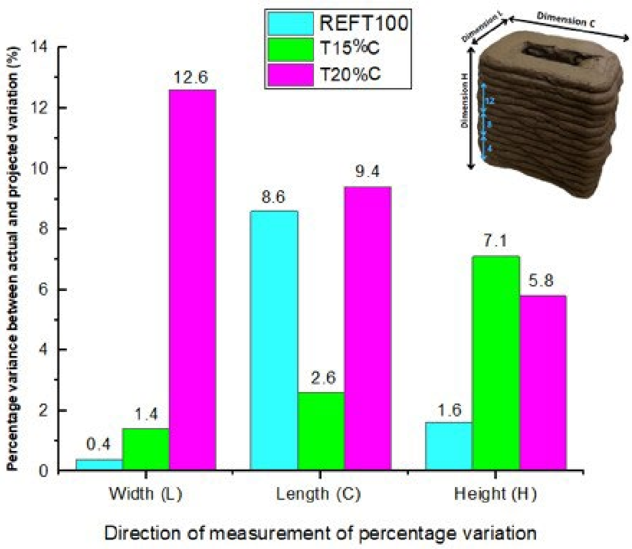

Figure 13. Direction of measurement of percentage variation of the printed soil-cement blocks.

The variations in width (L) and length (C) cannot be directly correlated to the composition of each mix. However, the height dimension (H) is a key indicator of the construction capacity of each mixture. The results in Figure 13 demonstrate that the reference mix (REFT100) exhibited the smallest percentage variation in height among the three mixes, with less than a 2% difference from the projected height. This is attributed to the higher cement content and lower water amount, enhancing particle cohesion and strength while minimizing deformations in the layers. Additionally, the results for T15%C and T20%C are in line with expectations, with the 20% cement content mixture displaying slightly lower dimensional variation in height compared to the 15% mixture.

3.4.2. Compressive strength of printed soil-cement blocks

Figure 14 illustrates that the reference block exhibits the highest strength among the three analyzed mixtures, which aligns with its higher cement content than the T20%C and T15%C mixtures. Despite using approximately six times less cement than the reference mix, the compressive strength is reduced by around 84% for the T15%C mix, with a cement consumption of 113.60 kg/cm³. In this instance, the compressive strength is only 16% of the reference strength.

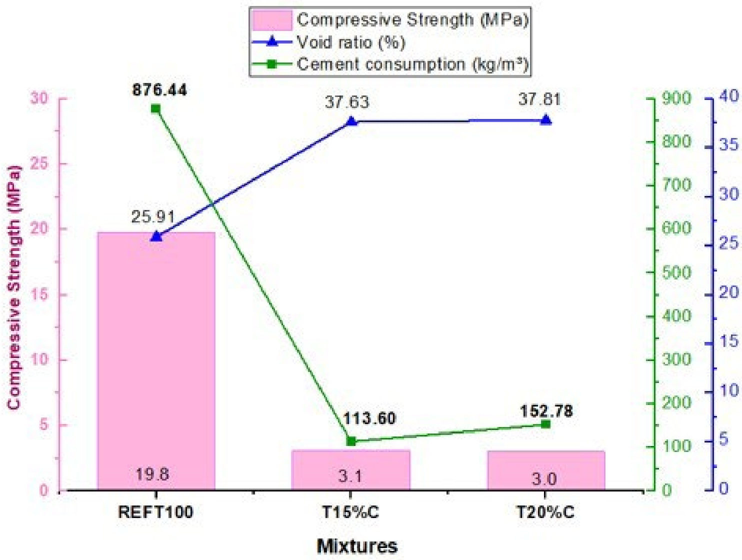

Figure 14. Compressive strength of printed soil-cement blocks.

The reduction in compressive strength of the T20%C mix is quite significant compared to the reference, similar to the result obtained for the mix with 15% cement. This suggests that the compositions with 15% (3.1 MPa) and 20% cement (3.0 MPa) have equivalent strengths, with no significant influence when only 5% of cement is reduced.

It's noteworthy that there are slight variations in the content of metakaolin and limestone filler in the two mixes. Just as with the cement content, these variations do not significantly impact the compressive strength in these compositions. Furthermore, the higher water demand of mixtures with additives leads to an increase in voids when part of the water is lost during curing, thereby reducing mechanical strength. The compressive strength results are also in line with those obtained for the void ratio of each mix. For the mixes with the highest voids, the compressive strength is lower because the voids present in the material decrease its density and, consequently, reduce its strength in its hardened state.

The reference mixture utilized in this study consists of a substantial amount of cement, specifically formulated with a 1:1 soil-to-cement ratio. This high proportion is responsible for the elevated compressive strength of the mixture. The choice of this ratio is necessitated by the limitations of the existing 3D printing system, which is designed exclusively to process and extrude mixtures characterized by a high paste content. However, the central objective of this article is to explore soil-cement blends with reduced cement content. To achieve this, traditional cement was substituted with metakaolin (MK) and limestone filler (LF), as elaborated in the methodology section. This modification aims to furnish the soil mixtures, which exhibit relatively low clay content, with adequate paste properties to facilitate successful 3D printing.

3.4.3. Axial compressive strength and flexural tensile strength of the specimens obtained from the blocks

Figure 15 displays the results of the flexural tensile test at 28 days in the X and Y directions. The test was performed on 40x40x160 mm pieces extracted from the printed blocks.

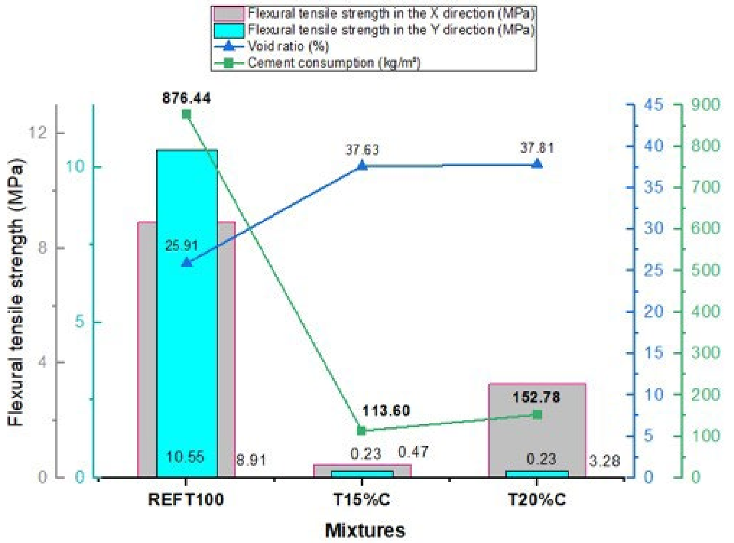

Figure 15. Flexural tensile strength of the samples extracted from the blocks.

It is apparent from the data that the reference mixture (REFT100) demonstrated higher flexural tensile strength in both directions compared to the T15%C and T20%C mixtures. Specifically, the Y direction exhibited the highest value at 10.55 MPa, while the X direction showed 8.91 MPa. In contrast, the T15%C and T20%C mixtures had flexural tensile strengths of 0.47 and 3.28 MPa, respectively, in the X direction. This indicates a reduction of 94.73% and 63.19% compared to the REFT100 mixture.

The flexural tensile strength and axial compressive strength at 28 days showed a decrease in both the X and Y directions for pieces measuring 40x40x160 mm extracted from the printed blocks.

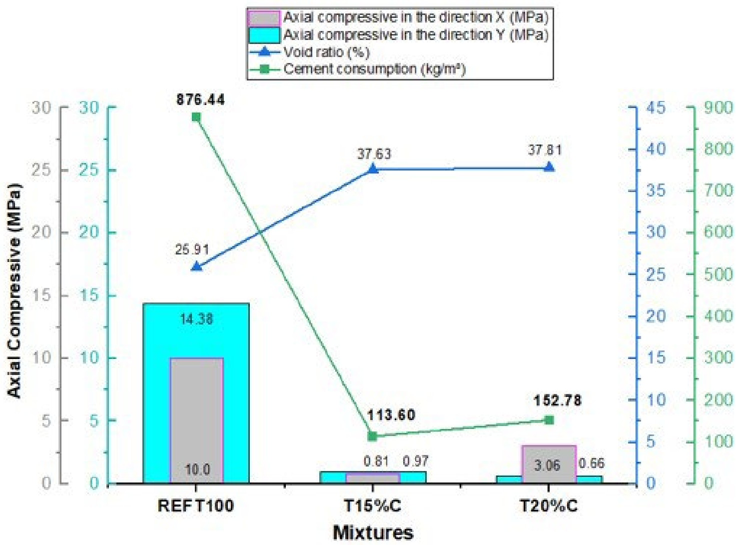

Figure 16. Axial compressive strength of the pieces extracted from the blocks.

The reference mix (REFT100) exhibited higher axial compressive strength in the X (10.0 MPa) and Y (14.38 MPa) directions, which can be attributed to the higher amount of cement in the mix. The T20%C mixture has a significant axial compressive strength of 3.06 MPa in the X direction (refer to Figure 16). This improved performance is attributed to the increased amount of cement (5%) and the addition of metakaolin, which alters the viscosity of the mixture and sustains strength through its pozzolanic activity.

The axial compression values of the T15%C mix indicated similar values in both directions: X (0.81 MPa) and Y (0.97 MPa). It is also apparent that reducing the amount of cement in the mixes leads to an increase in the void ratio, as the increase in the W/DMaterials ratio results in the formation of capillary voids. Thus, the mixtures T15%C (65%) and T20%C (60%) with higher limestone content demonstrate reduced strength gains and increased porosity in the hardened state. This is attributed to the high fineness of limestone, which does not promote a pozzolanic effect, unlike metakaolin, which possesses high fineness and acts chemically.

3.4.4. Specific mass, immersion water absorption and void ratio of the pieces extracted from the blocks

Figure 17 displays the specific mass, immersion water absorption, and void ratio values of the pieces extracted from the blocks.

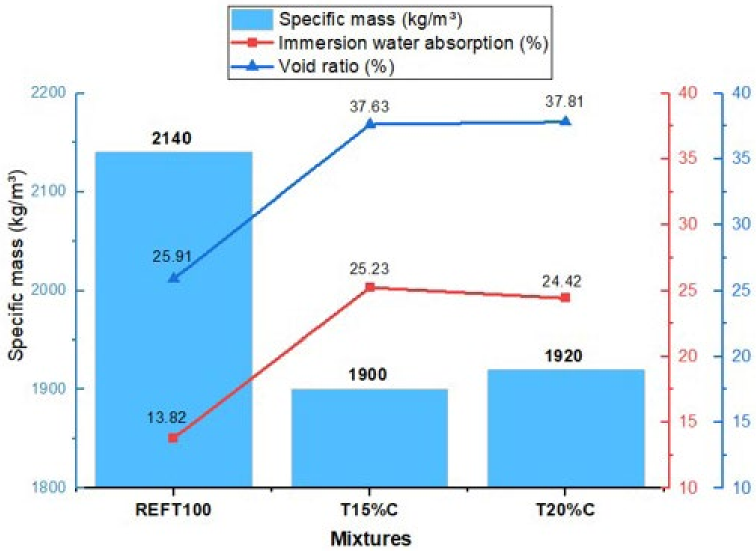

Figure 17. Specific mass, immersion water absorption, and void ratio of the pieces extracted from the blocks.

The results obtained for the void ratio for each mix align with those obtained for the specific mass. The decrease in the specific mass of the mixture, compared to the reference mix REFT100, can be attributed to the characteristics of each mineral addition, as these additions have lower specific masses than the cement used.

The considerable water content required for both the T15%C and T20%C mixtures significantly impacts the formation of voids, as a portion of this water evaporates post-mixture hardening without participating in cement hydration. Consequently, it was anticipated that mixtures with mineral additions and high water content would exhibit an increased voids index and a subsequent reduction in specific mass.

The increase in water absorption of each mixture is directly related to the increase in the void ratio. These voids allow water to pass through the material, favoring absorption.

In Figure 17, the graph indicates that the void ratio results show a 45.2% increase in T15%C and nearly 45.9% in T20%C compared to the reference. There is no significant difference in the voids between the two mixtures with mineral additions.

In terms of absorption, there is a more significant increase compared to the reference, with absorption reaching 82.6% for T15%C and 76.7% for T20%C. Additionally, there is a slightly greater difference between the two mixtures with additives in these results, with lower absorption in the 20% cement mix. This result can be attributed to the disparity in cement content, which is higher for the 20% mix. Consequently, the hydrated products of the cement promote the densification of the mixture, leading to a reduction in the interconnection between the pores.

4. CONCLUSIONS

The results presented allowed us to gain insight into the influence of various factors, including the incorporation of mineral additions such as metakaolin (MK) and limestone filler (LF), as well as the volume of paste and aggregate. Additionally, we examined the importance of the water to dry materials ratio on the viscosity and extrusion of the 3D soil-cement mixture, along with the potential reduction of the amount of cement as initially proposed.

1. In the buildability test, under printing conditions, the height of layers for the mixtures (REFT100, T15%C and T20%C) was found to be 16 layers.
2. The reference mix (REFT100) was deemed to have optimal printing conditions despite containing a lower volume of paste. This was attributed to the improved interaction between Portland cement and the chemical additives. The higher cement content facilitated better fluidity in the mix, resulting in a more cohesive spread.
3. The evaluation of printability was conducted using two distinct methodologies. The first approach employed a consistency table, which enabled the assessment of the distribution range of the mixture. The second method utilized the “sac-a-poche” technique, allowing for the simulation of the extrusion process prior to the actual printing procedure. This dual-method framework provided a comprehensive understanding of the material properties relevant to printability.
4. It was possible to reduce cement consumption in the T15%C (113.60 kg/m³) and T20%C (152.78 kg/m³) mixtures and make them printable. The reduction levels were 87.04% and 82.57%, respectively, compared to the reference mixture (876.44 kg/m³).
5. The incorporation of mineral additions like metakaolin significantly enhances viscosity and cohesion, both of which are crucial properties for applications such as 3D printing. These improvements are essential for achieving optimal printing performance and material behavior, highlighting the relevance of metakaolin in the context of advanced material formulations.
6. The block printed with the reference mix (REFT100) has the highest strength among the three analyzed mixes (19.8 MPa), which is consistent with the high cement content in the mix. The T15%C and T20%C mixtures, exhibit equivalent strengths (3 MPa);The compressive and bending stresses measured in the pieces extracted from the blocks show similar behavior to the blocks, with a decrease in strength as cement consumption is reduced.
7. Mixtures with mineral additions and high water content (T15%C and T20%C) have an increase in the void ratio and, consequently, a reduction in the specific mass. The increase in water absorption of each mixture is also directly related to the increase in the void ratio.
8. Better use of sandy-silt soil in the 3D printing process with earth would be made possible by providing this soil with desirable levels of clay, which would act as a natural binder in the mixture. However, as verified in this research, it is possible to use this soil in 3D printing of cement-stabilized earth, opting to replace it with mineral additions when high cement consumption is required.

Supplementary information ↑

Funding sources

Not applicable.

Supplementary material

Not applicable.

Data availability

Not applicable.

Acknowledgements

This work was partly financed by Fundação de Apoio à Pesquisa do Estado da Paraíba - FAPESQ, National Council for Scientific and Technological Development - CNPq, Intituto Federal da Paraíba -IFPB, and Coordenação de Aperfeiçoamento de Pessoal de Nível Superior do Brasil (CAPES).

Authorship contribution statement

Fernanda Morais Lima: Conceptualization, Data cleansing, Formal analysis, Research, Methodology, Visualization, Writing-original draft.

Marcos Alyssandro Soares dos Anjos: Conceptualization, Supervision, Methodology, Writing-review & editing.

Ilana Maria da Silva Barros: Supervision, Writing-review & editing.

Ueslei Silva Nunes: Supervision, Writing-review & editing.

Competing interests

The authors declare that they have no known financial conflicts of interest or personal relationships that could have influenced the work reported in this article.

Statement on the use of Artificial Intelligence

Not applicable.

REFERENCES

1. Rahal S, Kaci A, Skoudarli A. 2023. Evaluation of mechanical anisotropy induced by 3D printing process for earth-based materials. Mater. Today: Proc. S2214785323040622. https://doi.org/10.1016/j.matpr.2023.07.192

2. United Nations Environment Programme. 2024. Global status report for buildings and construction: beyond foundations: Mainstreaming sustainable solutions to cut emissions from the buildings sector. Accessed: Apr. 7, 2024. [Online]. https://doi.org/10.59117/20.500.11822/45095

3. Benachio GLF, Freitas MDCD, Tavares SF. 2020. Circular economy in the construction industry: A systematic literature review. J. Clean. Prod. 260:121046. https://doi.org/10.1016/j.jclepro.2020.121046

4. Bajpayee A, Farahbakhsh M, Zakira U, Pandey A, Ennab LA, Rybkowski Z, Dixit MK, Schwab PA, Kalantar N, Birgisson B, Banerjee S. 2020. In situ resource utilization and reconfiguration of soils into construction materials for the additive manufacturing of buildings. Front. Mater. 7:52. https://doi.org/10.3389/fmats.2020.00052

5. Ferretti E, Moretti M, Chiusoli A, Naldoni L, De Fabritiis, F, Visonà M. 2022. Mechanical properties of a 3D-printed wall segment made with an earthen mixture. Materials. 15(2):438. https://doi.org/10.3390/ma15020438

6. Faleschini F, Trento D, Masoomi M, Pellegrino C, Zanini MA. 2023. Sustainable mixes for 3D printing of earth-based constructions. Constr. Build. Mater. 398:132496. https://doi.org/10.1016/j.conbuildmat.2023.132496

7. Azeredo G, Morel JC, Lamarque CH. 2008. Applicability of rheometers to characterizing earth mortar behavior. Part I: experimental device and validation. Mater. Struct. 41:1465–1472. https://doi.org/10.1617/s11527-007-9343-9

8. Reyes AV, Gomaa M, Chatzivasileiadi A, Jabi W, Wardhana NM. 2018. Computing Craft - Early stage development of a robotically-supported 3D printing system for cob structures. In: 36th annual Education and Research in Computer Aided Architectural Design in Europe (eCAADe). 1:791-800. https://doi.org/10.52842/conf.ecaade.2018.1.791

9. Perrot A, Rangeard D, Courteille E. 2018. 3D printing of earth-based materials: Processing aspects. Constr. Build. Mater. 172:670–676. https://doi.org/10.1016/j.conbuildmat.2018.04.017

10. Gomaa M, Jabi W, Reyes AV, Soebarto V. 2021. 3D printing system for earth-based construction: Case study of cob. Autom. Constr. 124:103577. https://doi.org/10.1016/j.autcon.2021.103577

11. Dias LS, Anjos MAS, Barbosa MS, Bezerra UT. 2024. Evaluation of mix design parameters based on basic constitutive relationships for 3DCP printing. Cerâmica. 70:eZXBR6170. http://dx.doi.org/10.1590/ZXBR6170

12. Cardoso FA, John VM, Pileggi RG, Banfill PFG. 2014. Characterisation of rendering mortars by squeeze-flow and rotational rheometry. Cem. Concr. Res. 57:79–87. https://doi.org/10.1016/j.cemconres.2013.12.009

13. Cardoso FA, John VM, Pileggi RG. 2009. Rheological behavior of mortars under different squeezing rates. Cem. Concr. Res. 39(9):748–753. https://doi.org/10.1016/j.cemconres.2009.05.014

14. Gomaa M, Jabi W, Soebarto V, Xie YM. 2022. Digital manufacturing for earth construction: A critical review. J. Clean. Prod. 338:130630. https://doi.org/10.1016/j.jclepro.2022.130630

15. Chang, Y-C, Fiore D, Sevostianov F, Stirum G, Refalian G, Li Q, Riaz SR, Ye D. 2024. Digital Adobe. Institute for Advanced Architecture of Catalonia. Accessed: Jan. 15, 2024. [Online]. Retrieved from: https://iaac.net/project/digital-adobe

16. D'Haese R, Dubois V, Carpentier O, Chartier T, Chafei S, Wirquin E. 2018. Composite for additive manufacturing including flax by products and quarry fines. 2nd. Eur. Mag. Conf. BioComp. https://hal.science/hal-03263977

17. D'Haese, R, Carpentier O, Dubois V, Chafei, S, Wirquin E. 2022. 3D-printable materials made with industrial by-products: Formulation, fresh and hardened properties. Sustainability. 14(21):14236. https://doi.org/10.3390/su142114236

18. Soda PRK, Dwivedi A, M CS, Gupta S. 2024. Development of 3D printable stabilized earth-based construction materials using excavated soil: Evaluation of fresh and hardened properties. Sci. Total. Environ. 924:171654. https://doi.org/10.1016/j.scitotenv.2024.171654

19. Associação Brasileira de Normas Técnicas. 2016. ABNT NBR 7181: Solo - Análise granulométrica. ABNT, Rio de Janeiro.

20. Araújo RA, 2022. Avaliação de misturas cimentícias para impressão 3D com desempenho térmico otimizado. Tese (Doutorado em Ciência e Engenharia de Materiais) - Centro de Ciências Exatas e da Terra. Universidade Federal do Rio Grande do Norte. Natal – RN.

21. Diniz HAA, Martinelli AE, Cabral KC, Ferreira RLDS, Da Silva IFD. 2023. Synergistic effects of the use of metakaolin, sand and water on the properties of cementitious composites for 3D printing. Constr. Build. Mater. 366:130277. https://doi.org/10.1016/j.conbuildmat.2022.130277

22. Associação Brasileira de Normas Técnicas. 2009. ABNT NBR NM 52: Agregado miúdo – Determinação da massa específica e massa específica aparente. ABNT, Rio de Janeiro.

23. Associação Brasileira de Normas Técnicas. 2009. ABNT NBR NM 53: Agregado graúdo – Determinação da massa específica, massa específica aparente e absorção de água. ABNT, Rio de Janeiro.

24. Associação Brasileira de Normas Técnicas. 2006. ABNT NBR NM 45: Agregados - Determinação da massa unitária e do volume de vazios. ABNT, Rio de Janeiro.

25. Associação Brasileira de Normas Técnicas. 2016. ABNT NBR 13276: Argamassa para assentamento e revestimento de paredes e tetos – Determinação do índice de consistência. ABNT, Rio de Janeiro.

26. International Organization for Standardization. 2023. ISO/ASTM FDIS 52939: Additive manufacturing for construction — Qualification principles — Structural and infrastructure elements. International Organization for Standardization.

27. Associação Brasileira de Normas Técnicas. 2012. ABNT NBR 8492: Tijolo de solo-cimento – Análise dimensional, determinação da resistência à compressão e da absorção de água - Método de ensaio. ABNT, Rio de Janeiro.

28. Nunes GM, Anjos MAS, Lins ABSM, Negreiros AMS, Pessoa LR. 2023. Evaluation of the mechanical behaviour of representative volumetric elements of 3DCP masonry mixtures with partial replacement of cement by limestone filler and metakaolin. J. Build. Eng. 78:107650. https://doi.org/10.1016/j.jobe.2023.107650

29. Associação Brasileira de Normas Técnicas. 2005. ABNT NBR 13279: Argamassa para assentamento e revestimento de paredes e tetos - Determinação da resistência à tração na flexão e à compressão. ABNT, Rio de Janeiro.

30. Associação Brasileira de Normas Técnicas. 2009. ABNT NBR 9778: Argamassa e concreto endurecidos - Determinação da absorção de água, índice de vazios e massa específica. ABNT, Rio de Janeiro.

31. Lahbabi S, Bouferra R, Saadi L, Khalil A. 2024. Study of the physicochemical, mineralogical, and geotechnical properties of clayey soils to improve the durability of eco-construction materials in the rural region. Constr. Build. Mater. 411:134304. https://doi.org/10.1016/j.conbuildmat.2023.134304

32. Silva G, Ñañez, R, Zavaleta D, Burgos V, Kim S, Ruiz G, Pando MA, Aguilar R, Nakamatsu J. 2022. Eco-friendly additive construction: Analysis of the printability of earthen-based matrices stabilized with potato starch gel and sisal fibers. Constr. Build. Mater. 347:128556. https://doi.org/10.1016/j.conbuildmat.2022.128556

33. Davey BG, Russell JD, Wilson MJ. 1975. Iron oxide and clay minerals and their relation to colours of red and yellow podzolic soils near Sydney, Australia. Geoderma. 14(2):125–138. https://doi.org/10.1016/0016-7061(75)90071-3

34. Muñoz PV, Morales MPO, Letelier VG, Mendívil MAG. 2016. Fired clay bricks made by adding wastes: Assessment of the impact on physical, mechanical and thermal properties. Constr. Build. Mater. 125:241–252. https://doi.org/10.1016/j.conbuildmat.2016.08.024

35. Boukili GE, Lechheb M, Ouakarrouch M, Dekayir A, Kifani-Sahban F, Khaldoun A. 2021. Mineralogical, physico-chemical and technological characterization of clay from Bensmim (Morocco): Suitability for building application. Constr. Build. Mater. 280:122300. https://doi.org/10.1016/j.conbuildmat.2021.122300

36. Gol F, Saritas ZG, Cıbuk S, Ture C, Kacar E, Yilmaz A, Arslan M, Sen F. 2022. Coloring effect of iron oxide content on ceramic glazes and their comparison with the similar waste containing materials. Ceram. Int. 48(2):2241–2249. https://doi.org/10.1016/j.ceramint.2021.10.001

37. Tay YWD, Qian Y, Tan MJ. 2019. Printability region for 3D concrete printing using slump and slump flow test. Compos. Part B Eng. 174:106968. https://doi.org/10.1016/j.compositesb.2019.106968

38. Ma G, Li Z, Wang L. 2018. Printable properties of cementitious material containing copper tailings for extrusion based 3D printing. Constr. Build. Mater. 162:613–627. https://doi.org/10.1016/j.conbuildmat.2017.12.051

39. Shah V, Parashar A, Mishra G, Medepalli S, Krishnan S, Bishnoi S. 2020. Influence of cement replacement by limestone calcined clay pozzolan on the engineering properties of mortar and concrete. Adv. Cem. Res. 32(3):101–111. https://doi.org/10.1680/jadcr.18.00073

40. Sabino TDDMM, Nunes US, Marinho GS, Freitas JCDO, Martinelli AE, Da Nóbrega ACV. 2024. Limestone calcined clay cement (LC3) coating mortars as an energy-efficient option for construction. Constr. Build. Mater. 437:136954. https://doi.org/10.1016/j.conbuildmat.2024.136954

41. Avet F, Sofia L, Scrivener K. 2019. Concrete performance of limestone calcined clay cement (LC^3) compared with conventional cements. Adv. Civ. Eng. Mater. 8(3):275–286. https://doi.org/10.1520/ACEM20190052

42. Araújo RA, Martinelli AE, Cabral KC, Dantas AFOA, Silva IFD, Xavier AAC, Santos AL. 2022. Thermal performance of cement-leca composites for 3D printing. Constr. Build. Mater. 349:128771. https://doi.org/10.1016/j.conbuildmat.2022.128771